CHAPTER VI

THERMAL DESIGN

By Earl C. Hastings, Jr., Richard E. Turner,
and G. Louis Smith
Langley Research Center

SECTION I - INTRODUCTION

An essential phase of the Explorer XIII development was a thermal study and design to provide an acceptable temperature environment for the electronics components and external surfaces of the satellite during ascent and in orbit. It was necessary to establish by preflight analysis and tests that tolerable temperatures could be maintained in three regimes of flight. In the first regime (from launch until release of the heat shield) the satellite was subjected to radiative and conductive heat from the shield. In the second regime, after release of the shield at 350,000 feet, the satellite was heated by free molecular flow. In the third regime - the orbit phase - it was necessary that temperatures within limits for a 1-year lifetime be established. In addition to these three regimes, a study was made to investigate the effect of elevated rocket-motor temperatures during launch and after burnout.

This chapter will deal with some pertinent preflight estimates and correlation of these estimates with flight data.

SECTION II - SYMBOLS

a_s	absorptivity of solar radiation
a	semimajor axis of orbit, ft
A	cross-sectional area of satellite section, ft^2
B	decay constant for atmosphere, taken as 3.48×10^{-5}/ft
E	eccentric anomaly
erf	error function
g_o	acceleration due to gravity at earth's surface
$I_n( )$	modified Bessel function of the first kind of order n
k	Boltzmann constant, 0.728×10^{-26} Btu/molecule-^oR

n number of molecules striking surface per unit area per unit time

N number of molecules per unit volume

P orbit period, min

q heat-transfer rate per unit surface area, Btu/ft^2-sec

Q heat input per unit surface area per orbit, Btu/ft^2-orbit

$\overline{Q}$ total heat input to satellite section, Btu/ft^2-orbit

r spacecraft distance from center of earth, ft

r_0 reference altitude, ft

R_e radius of the earth, 2.0903×10^7 ft

$s = \frac{U}{\bar{v}}$

S total surface area of satellite sector, ft^2

t time, min

T temperature, ^oR

T_∞ free-stream temperature, ^oR

U free-stream velocity, ft/sec

$\bar{v}$ mean molecular velocity, ft/sec

x argument of Bessel function

α thermal accommodation coefficient

β angle between flow direction and the normal to the surface, deg

γ ratio of specific heats

ϵ orbit eccentricity

ϵ_{TH} total hemispherical emissivity

$\eta = s \cos \beta$

$\mu = g_o R_e^2$, 1.42×10^{16} ft^3/sec^2

σ Stefan-Boltzmann constant, 2.0×10^{-13} $\frac{\text{Btu}}{\text{in.}^2\text{-min-}^\circ\text{R}^4}$

Subscripts:

av average

m mean

p perigee

w wall

SECTION III - ANALYTICAL METHODS

Methods were established by which analytical solutions to the heat-transfer problems could be found for all the regimes discussed. These are derived and discussed in detail in reference VI-1 and are not repeated herein. Reference VI-1 also contains detailed discussions of the test results and coatings evaluated in this thermal-design study. The estimates discussed herein have been performed for the actual launch date of Explorer XIII (August 25, 1961); however, the estimates of reference VI-1 consider a launch data of June 15, 1961.

SECTION IV - RESULTS AND DISCUSSION

Estimated temperatures.- The temperature limits specified for Explorer XIII are tabulated as follows: (These limits had been established by the designers as those which might impair reliability or proper operation of the sensors.)

Component	Maximum allowable temperature, $^\circ$F	Minimum allowable temperature, $^\circ$F
Telemetry	120	15
Pressurized cells	250	-50
Steel-covered-grid detectors	180	-100
Copper-wire-card detectors	300	None given
Solar cells	250	-50
Cadmium-sulfide cells	200	None given
Impact detectors	250	-50

Estimated heating calculations during ascent and in orbit to be discussed herein were based on the nominal trajectory defined as follows:

Launch characteristics:

Actual launch date	August 25, 1961
Launch azimuth	90° from north
Launch elevation, deg	79.88

Orbital characteristics:

Initial perigee altitude, n.m.	207
Initial apogee altitude, n.m.	527
Orbit period, min	98
Orbit inclination, deg	37.68
Satellite lifetime, year	>1

Prior to the launch of Explorer XIII, several nominal trajectories were considered. For this reason the values listed in this table differ slightly from the predicted orbital parameters in table II-4. Studies have established that these differences would not have a large effect on the data discussed in the present chapter.

Figure VI-1 shows a sketch of Explorer XIII in the heat shield. Temperatures were estimated during ascent for three stations on the heat shield: the stagnation point of the hemispherical tip, the conical section, and the cylindrical section (designated by 1, 2, and 3, respectively, in fig. VI-1). Both outside- and inside-wall temperatures were computed for station 3 on the cylindrical section which was located approximately over the first row of pressure cells. The temperature history of the pressure cells due to this radiant heating source was also estimated and the results are plotted in figure VI-2.

During simulated ascent, experimental values of payload temperature were obtained as part of the heat-shield qualification tests. The Explorer XIII prototype was placed inside the heat shield and the shield was subjected to the estimated outside-wall-temperature time histories of figure VI-2. Temperatures of the spacecraft during the test were monitored by a number of thermocouples on the exposed surfaces and in the telemetry canisters. Results of this test are

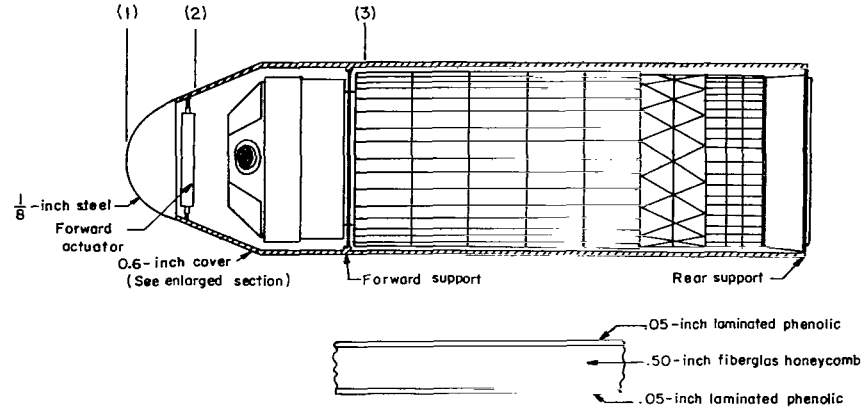

Figure VI-1.- Explorer XIII in heat shield.

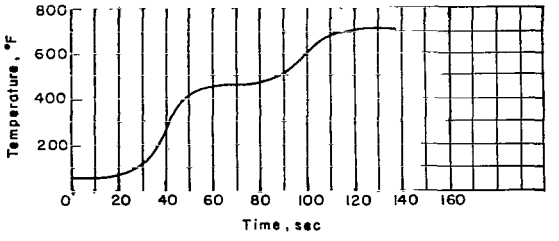

(a) Temperature time history at station 1.

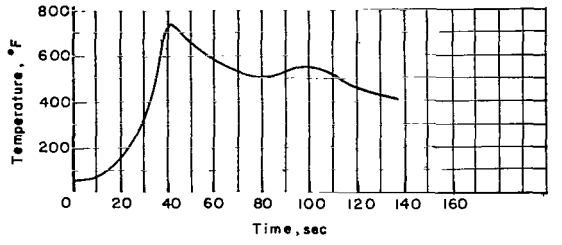

(b) Temperature time history at station 2.

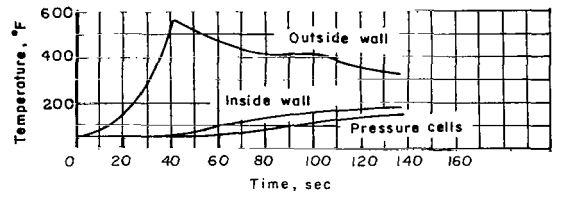

(c) Temperature time history at station 3.

Figure VI-2.- Temperatures during ascent with heat shield in place.

presented in figure VI-3 along with pressure-cell estimates from figure VI-2 which are shown for comparison.

It can be seen from figure VI-3 that the maximum temperature of the pressure cells from the simulated ascent test was considerably lower than that predicted, and that the steel-covered-grid detectors and copper-wire-card detectors experienced temperature rises of less than 20° F during the test. Although not shown in the figure, values of telemetry-canister temperature remained constant throughout the test. It was not expected that these components would respond to external temperature sources over such a relatively short time. The analytical and experimental studies conducted in this part of the thermal-design program established that during ascent with the heat shield on, the external surfaces of the satellite would remain within tolerable temperature limits and that the telemetry temperature would not be affected by aerodynamic heating.

The method discussed in reference VI-1 was used to estimate the free-molecular flow heating for Explorer XIII after heat-shield ejection for a range of altitudes between 300,000 and 400,000 feet. These estimates were made only for the pressure cells, since they would heat most rapidly because of their surface characteristics. This study indicated that above 350,000 feet, there would be no increase in detector temperature due to this heating source for flow parallel to the flight path.

Since the last stage of the booster vehicle was an integral part of Explorer XIII, it was necessary to evaluate the effects of elevated temperatures of this booster stage on the various detectors of the satellite. Figure VI-4 shows experimentally determined temperature histories from the static firing of a rocket motor similar to the last stage of the Scout launch vehicle at reduced external pressures (ref. VI-2). These data indicate that following burning of the last stage the temperatures of the rocket-motor case generally reached maximum values at or before 500 seconds after ignition and then decreased with increasing time.

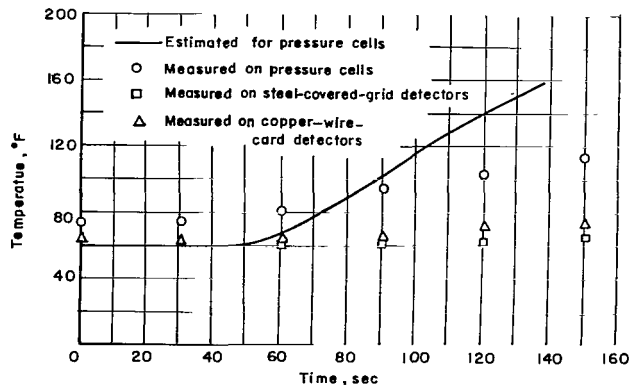

Figure VI-3.- Estimated and measured spacecraft temperatures during simulated ascent heating test.

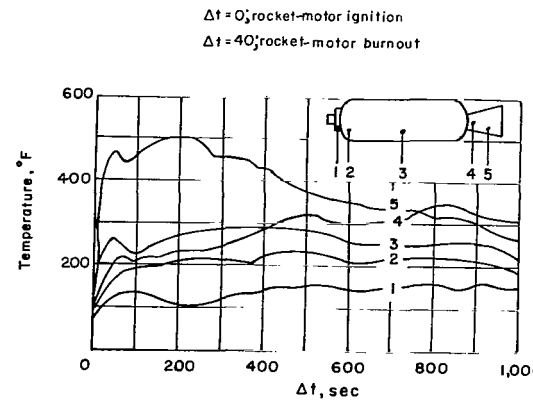

Figure VI-4.- Measured temperatures from static firing of the X248-A9 rocket motor.

An analytical program was used to consider the influence of the nozzle temperature (point 5) and the motor-case temperature (point 3) on the rear row of pressure cells and the steel-covered-grid detectors and copper-wire-card detectors. To be conservative, a constant temperature of 600° F at point 5 and a constant temperature of 400° F at point 3 were assumed to exist from Δt = 0 minute to Δt = 20 minutes. Direct and reflected solar radiation and earth thermal radiation were also considered in these calculations. The results are shown in figure VI-5.

These data show a constant increase in the temperature of the steel-covered-grid detectors after Δt = 4 minutes reaching a value of 144° F when the satellite enters the earth's shadow at Δt = 20 minutes. After Δt = 20 minutes the temperatures will decrease since the solar-heating input is removed. The temperatures of the copper-wire-card detectors and last row of pressure cells are 118° F and 125° F, respectively, at this time. The temperature values computed for the last row of pressure cells should be representative of all the pressure cells because of the excellent thermal conductivity of the pressurized-cell mounting structure and the existence of a heating source from the support at the rocket-motor headcap. Estimates were also made to determine the increase in telemetry temperature associated with a constant headcap temperature of 200° F for 20 minutes. These estimates established that a rise of less than 5° F would result from this heating source.

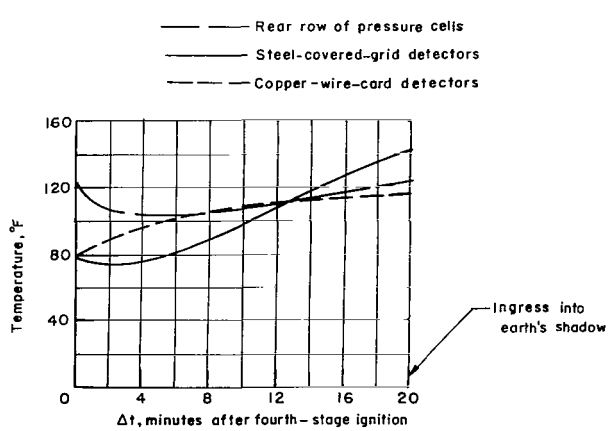

Figure VI-5.- Estimated satellite surface temperature due to last stage rocket-motor heating.

This phase of the study established that of all the heating sources

investigated during ascent, the effects of the rocket-motor temperatures had most pronounced effects on the detectors. All the detector temperatures were found to remain within tolerable limits; however, the increase in telemetry temperature was expected to be less than 5° F from the ascent heating sources.

Orbital heating calculations were performed on an electronic data processing machine which computed 12 time-dependent temperatures simultaneously. The satellite was considered to be composed of a number of sectors with the heat-flow paths shown in the schematic diagram below:

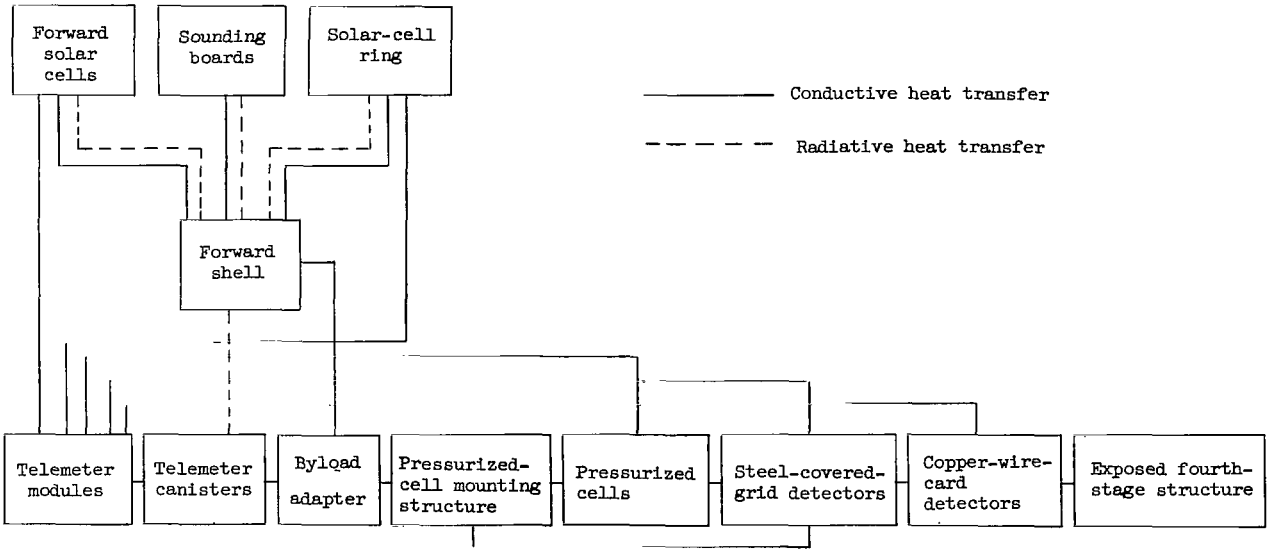

Passive thermal design was used, and heat-flux equations were written for each of the sectors by considering conductive and radiative heat transfer between the sectors, and where necessary direct and reflected solar radiation and earth thermal radiation were considered. (See ref. VI-1.)

The following are the absorptivity and emissivity values of the exposed sectors of the satellite:

Component	Absorptivity, α_s	Emissivity, ϵ_{TH}	Surface finish*
Forward shell	0.71	0.42	410 stainless steel; sand blasted with 100 mesh grit; heated in air at 600° F for 5 minutes
Sounding boards	.71	.42	Same as above
Composite solar cell ring	.57	.79	Black and white mosaic
Composite solar cells on forward face	.41	.89	Black and white mosaic
Pressurized cells	.19	.16	Vapor-deposited aluminum and silicon monoxide films
Steel-covered-grid detectors	.32	.82	Lusterless white enamel
Copper-wire-card detectors	.66	.69	Enameled copper wire
Exposed fourth-stage structure	.93	.74	Black lacquer

*For details of surface finishes, see ref. VI-1.

Interior surfaces were prepared with low-emissivity coatings to reduce heat transfer from the motor case. The last stage rocket motor and the satellite surfaces which were exposed to radiation from the motor case were covered with aluminum foil. The mounting bulkhead, the inside of the forward shell, and the outside of telemeter canisters, and the bases were gold plated.

Since there was no system on Explorer XIII to orient the spacecraft it was necessary to consider temperatures both for the mode of spin about the principal axis (the condition at injection into orbit), which will be referred to herein as the "stable" mode, and for the mode of spin about the axis of maximum moment of inertia, referred to herein as the "tumbling" mode. Studies indicated that the initial spin motion should convert to a tumbling motion in less than 2 weeks as shown in figure VI-6. The first computations of orbital temperatures were made for the tumbling mode since the hottest and coldest cases could be made to occur in this mode with proper selection of launch time. Estimates discussed in reference VI-1 establish that for the coatings used, telemetry-temperature values for Explorer XIII in the tumbling mode should be between 30° F and 111° F for a 1-year lifetime.

A study of the parameters governing the launch time (stable mode of spin) established that for an August 25 launch date, the hours between 0900 and 1330 e.s.t. were satisfactory. Figure VI-7 is an estimated temperature time history of the sensors for a 1330 e.s.t. launch. The telemetry temperature of 51.6° F during orbital heating is also noted. Figure VI-8 shows calculated percent-time-in-sunlight histories for three launch times on August 25.

Flight-test results.- Explorer XIII was instrumented with 18 thermistors to measure temperatures in flight (fig. VI-9). Solar-cell temperatures were measured under the mounting frames of two units 180° apart on the heat-transfer band. Forward-shell temperatures were measured on the inside wall of the cylindrical section, also at stations 180° apart. Two of the 0.002-inch-thick pressure cells in the first row had thermistors mounted on the bottom of their base plates. The steel-covered-grid detectors had four thermistors (spaced 90° apart) located directly under the steel grids. Two wire-card-detector temperatures were measured in the fiber-glass backing under individual cards. Thermistors located in each of the telemeter stacks (in the second module forward of the base) were used to measure telemetry temperature. The cadmium-sulfide cells had thermistors located inside the flask below the light-sensing element.

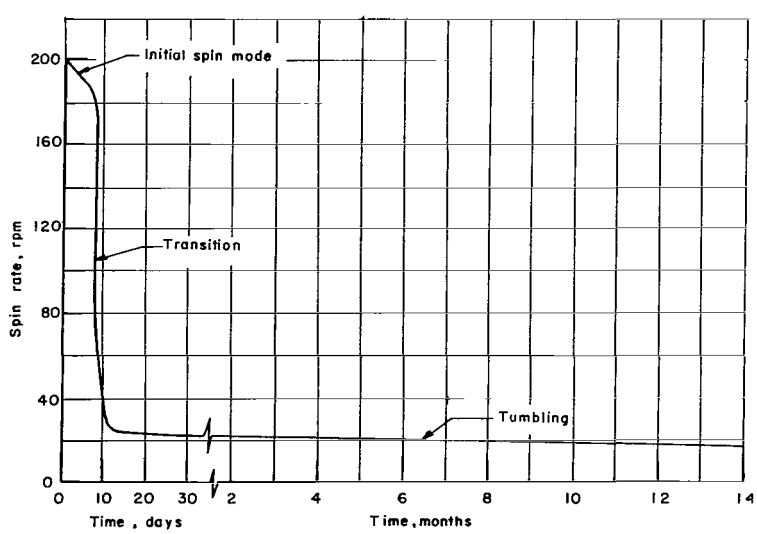

Figure VI-6.- History of spin rate due to magnetic torques.

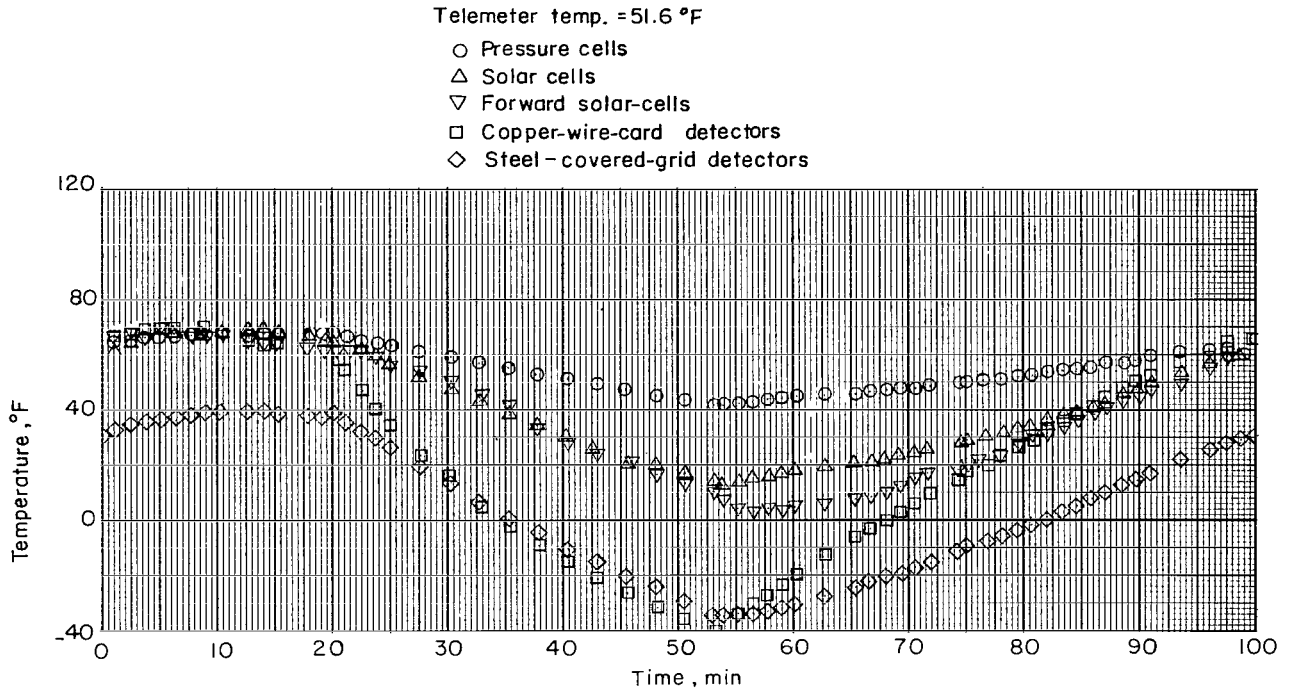

Figure VI-7.- Calculated temperature history for the stable satellite launched 1330 on August 25, 1961.

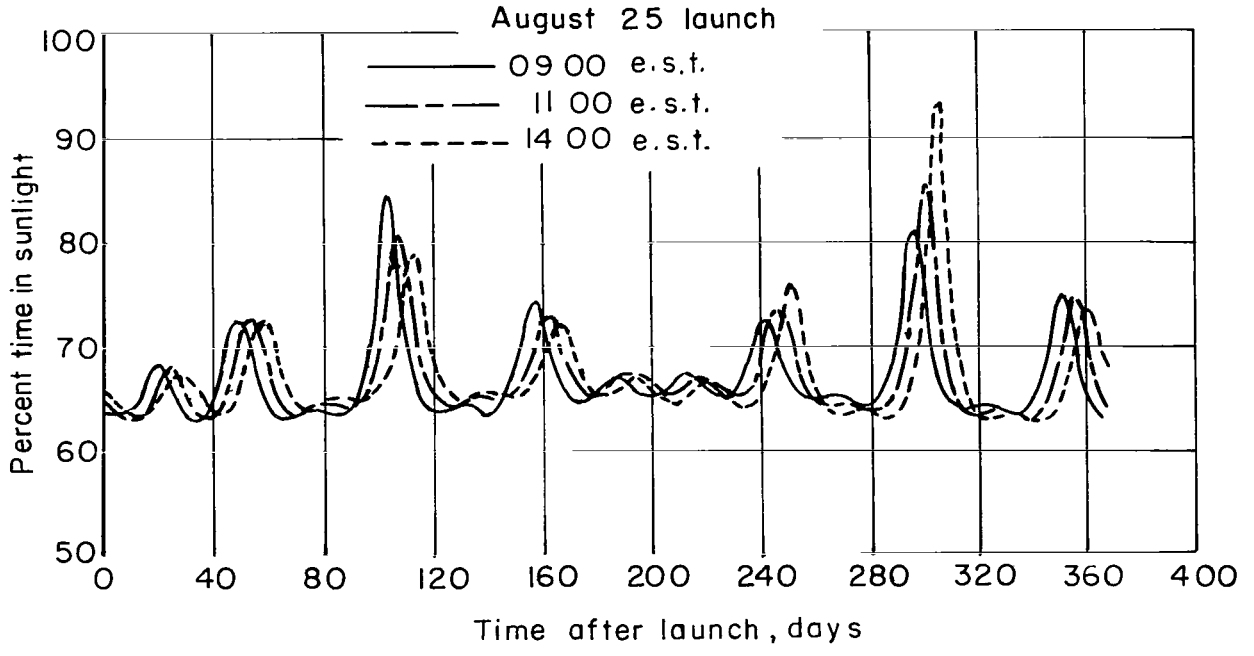

Figure VI-8.- Percent time in sunlight as a function of days after launch.

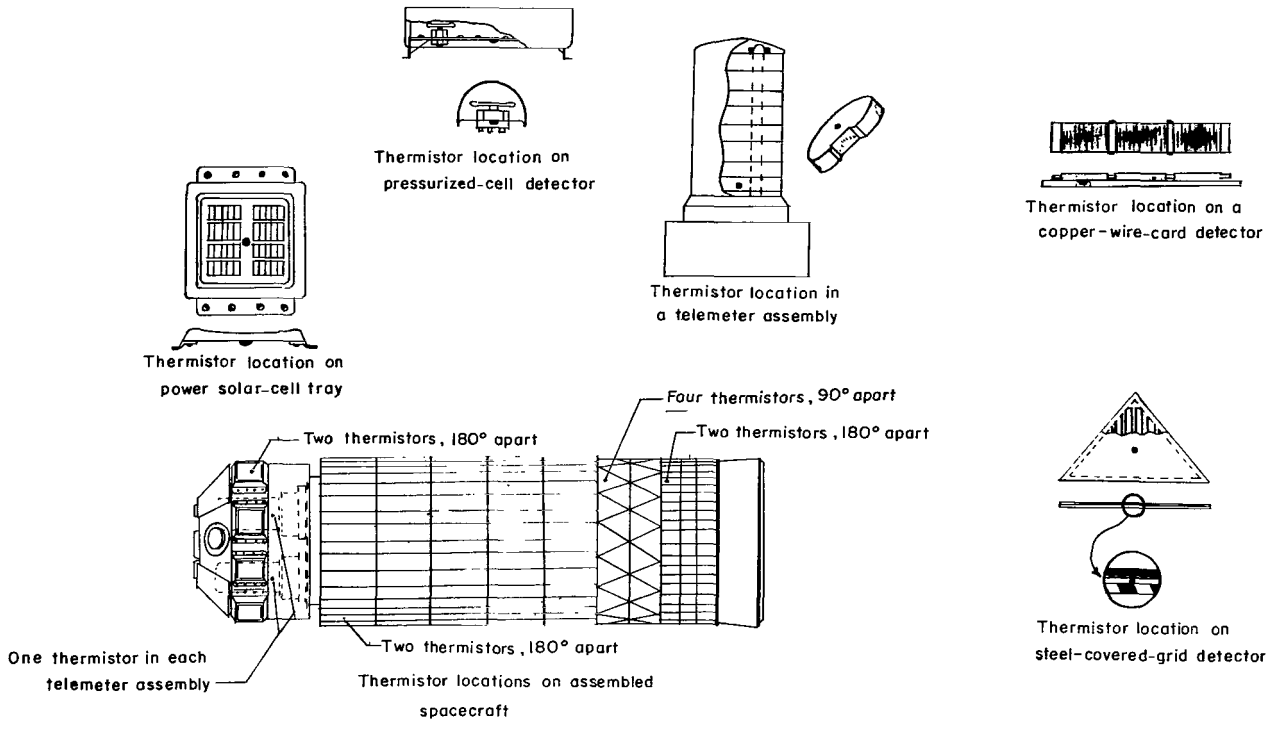

Figure VI-9.- Thermistor locations.

Temperature data during orbit were obtained by interrogating the satellite as it passed the stations of the Minitrack network. Since temperature data were not stored by the satellite, values recorded during an interrogation represented temperatures only at the time of the interrogation so that the orbital-temperature cycle could not be read out directly. No temperature data were transmitted during ascent.

Recorded flight-temperature data for about 46 hours after launch are shown in figure VI-10. Also shown in figure VI-10 are maximum orbit heating values of temperatures from figure VI-7. In figures VI-10(c) and (d) maximum estimated ascent heating values of temperature (from fig. VI-5) are shown for the pressurized cells and telemeter packs. These latter values were taken as constant from 8 to 46 hours. The flight-data value at $\Delta t = 0$ was a prefiring value taken with the satellite inside the heat shield prior to launch. Flight-test-temperature data for the copper-wire-card detectors and cadmium-sulfide cells are discussed in chapters X and XI and are therefore omitted from figure VI-10. Steel-covered-grid-detector temperatures are also omitted, since these data are presented in reference VI-3. Figure VI-10 indicates that at the first interrogation at about 1.5 hours, temperatures were generally close to the estimated value for the ascent heating effects, which indicates reasonable estimates for the ascent heating effects. Measured telemeter temperatures were 6° F higher than prelaunch at the first interrogation. Later interrogations show that all the flight data are near to, or greater than the maximum expected orbital heating values from figure VI-7.

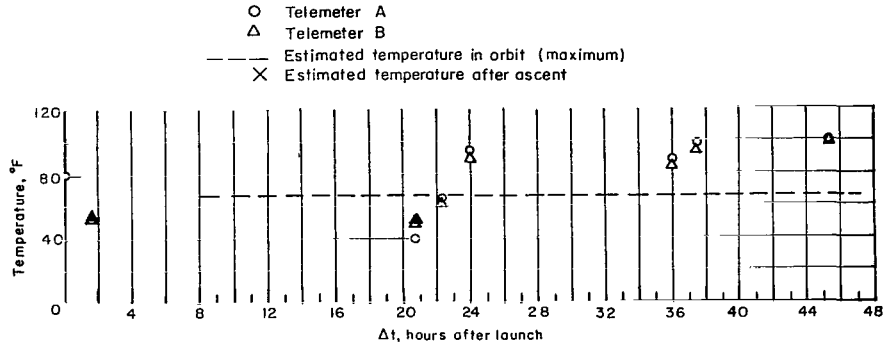

(a) Forward-shell temperatures.

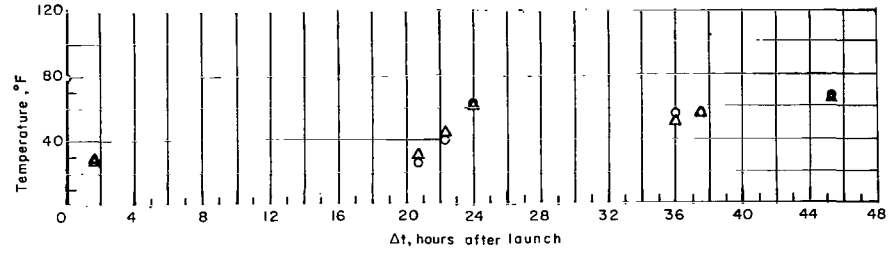

(b) Solar-cell temperatures.

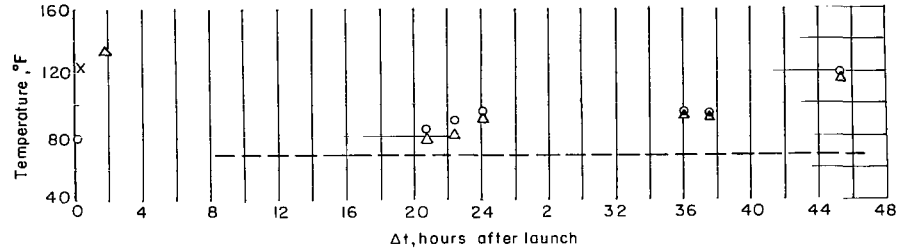

(c) Pressurized-cell temperatures.

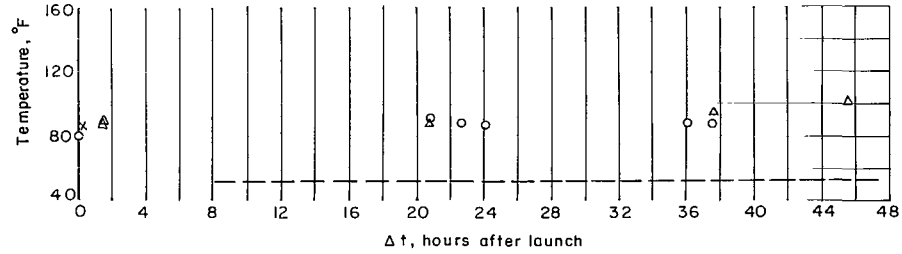

(d) Telemeter temperatures.

Figure VI-10.- Comparison of estimated and measured temperatures from Explorer XIII.

Since the orbit of Explorer XIII was known to be different from the nominal orbit used for the estimates, an investigation was made to study the orbital heating effects of free molecular flow resulting from the low perigee. The method employed was to determine the total free-molecular-flow heat input for various orientations of the satellite at perigee passage and to reduce this to a surface-temperature increase.

The aerodynamic heat-transfer rate to a body in free molecular flow is given by the corrected form of an equation in reference VI-4 as

$$\frac{q}{\alpha N k T_\infty U} = -\frac{\gamma + 1}{2(\gamma - 1)} \frac{n}{N\bar{v}s} \frac{T_w}{T_\infty} + \left(s^2 + \frac{\gamma}{\gamma - 1}\right)\frac{n}{N\bar{v}s} - \frac{e^{-\eta^2}}{4s\sqrt{\pi}} \tag{1}$$

where n is given by

$$n = \frac{N\bar{v}}{2\sqrt{\pi}}\left[e^{-\eta^2} + \sqrt{\pi}\eta(1 + \operatorname{erf}\eta)\right] \tag{2}$$

For satellite velocities, $s \gg 1$ so that $e^{-\eta^2} \to 0$ and $\operatorname{erf}\eta \to 1$ for $\cos\beta \to 0$. For $\cos\beta < 0$, $\operatorname{erf}\eta \to -1$ so that equation (2) becomes

$$n = NU\cos^*\beta \tag{3}$$

where

$$\cos^*\beta = \cos\beta \quad \text{for} \quad \cos\beta > 0$$

$$\cos^*\beta = 0 \quad \text{for} \quad \cos\beta < 0$$

The second term on the right-hand side of equation (1) predominates, so that equation (1) reduces to

$$q = \alpha\left(\frac{NkT_\infty}{\bar{v}^2}\right)U^3\cos^*\beta \tag{4}$$

The atmospheric term is fitted to an exponential variation of geocentric radius

$$\frac{NkT_\infty}{\bar{v}^2} = \left(\frac{NkT_\infty}{\bar{v}^2}\right)_{r_0} e^{-B(r-r_0)} \tag{5}$$

where r_0 is the reference altitude. Thus the heating rate on a flat-plate element is

$$q = \alpha\left(\frac{NkT_\infty}{\bar{v}^2}\right)_{r_0} U^3\cos^*\beta e^{-B(r-r_0)} \tag{6}$$

Orbit mechanics give the equations (ref. VI-5):

$$r = a(1 - \epsilon \cos E) \tag{7}$$

$$U^2 = \frac{\mu\left(1 + \epsilon \cos E\right)}{a\left(1 - \epsilon \cos E\right)} \tag{8}$$

$$\frac{dE}{dt} = \frac{\mu^{1/2}}{a^{3/2}(1 - \epsilon \cos E)} \tag{9}$$

The total aerodynamic-heating input to a flat-plate element of unit area during one orbital pass is then

$$Q = \int_0^P q \, dt = \oint \frac{q \, dE}{dE/dt}$$

$$= \alpha\mu\left(\frac{NkT_\infty}{\bar{v}^2}\right)_{r_0} e^{-B(a-r_0)} \oint \cos^*\beta(E) e^{Ba\epsilon \cos E} \times \left[1 + 2\epsilon \cos E + O\left(\epsilon^2\right)\right] dE \tag{10}$$

Now, assume $\cos^*\beta$ is constant, and with the relations from reference VI-6 that

$$\oint e^{x \cos E} dE = 2\pi I_0(x)$$

and

$$\oint \cos E e^{x \cos E} dE = 2\pi I_1(x)$$

equation (10) becomes

$$Q = 2\pi\alpha\mu\left(\frac{NkT_\infty}{\bar{v}^2}\right)_{r_0} e^{-B(a-r_0)} \cos^*\beta\left[I_0(Ba\epsilon) + 2\epsilon I_1(Ba\epsilon) + O\left(\epsilon^2\right)\right] \tag{11}$$

For large values of x

$$I_n(x) \approx \frac{e^x}{\sqrt{2\pi x}}$$

so that, choosing $r_0 = r_p$, equation (11) can be written as

$$Q = \alpha\mu\left(\frac{NkT_\infty}{\bar{v}^2}\right)_{r_p} \cos^*\beta\sqrt{\frac{2\pi}{Ba\epsilon}}\left[1 + 2\epsilon + O\left(\epsilon^2\right)\right] \tag{12}$$

Consider the case where the satellite is assumed to enter perigee broadside ($\beta = 0^o$). Integrating Q over the surface and denoting the cross-sectional area as A, the total aerodynamic-heating input in one orbit is

$$\bar{Q} = \alpha A\mu\left(\frac{NkT_\infty}{\bar{v}^2}\right)_{r_p}\sqrt{\frac{2\pi}{Ba\epsilon}}\left[1 + 2\epsilon + O\left(\epsilon^2\right)\right] \tag{13}$$

The resulting mean temperature is determined by the following considerations: Neglecting the aerodynamic heating, the satellite will be at a mean temperature T_m, and will thus be radiating heat at a rate $S\epsilon_{TH}\sigma T_m^4$, so that the total heat radiated during the orbit is $PS\epsilon_{TH}\sigma T_m^4$. This is also the radiative heat input. With aerodynamic heating, the temperature will increase to a value T_1 such that

$$PS\epsilon_{TH}\sigma T_1^4 = PS\epsilon_{TH}\sigma T_m^4 + \bar{Q} \tag{14}$$

Hence the temperature is found to be

$$T_1 = \left(T_m^4 + \frac{\bar{Q}}{PS\epsilon_{TH}\sigma}\right)^{1/4} \tag{15}$$

The approximation is intrinsically made that $\left(T_{av}\right)^4 = \left(T^4\right)_{av}$, which is valid for reasonable temperature fluctuations.

This method of analysis was applied to a cylinder having the properties of the pressure-cell sector and the estimated-temperature time histories for four different orientation angles are shown in figure VI-11. Atmospheric properties from reference VI-7 were used in these calculations.

Also plotted in figure VI-11 is a line representing the measured pressure-cell temperatures shown in figure VI-10. It can be seen that the flight temperatures lie within the calculated temperatures for values of β between about 60^o and 80^o. Although the calculated time histories shown in figure VI-11 are somewhat questionable because of uncertainties in atmospheric data at the higher altitudes, they do serve to illustrate that the addition of the free-molecular-flow heating effects were sufficient to cause the elevated flight temperatures encountered.

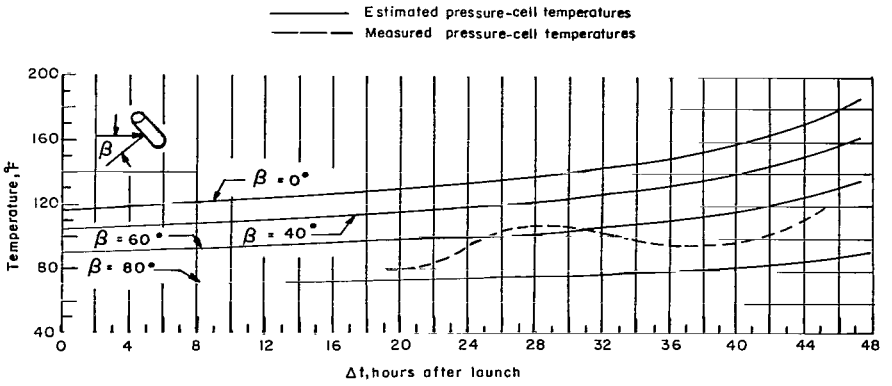

Figure VI-11.- Estimated and measured pressure-cell temperatures for Explorer XIII.

This analysis was applied to the pressure cells since it had been previously established by ground tests that the telemetry temperature in orbit would be controlled by the mean temperature of the pressure cells. It is felt, therefore, that the high flight temperatures on the pressure cells were caused by free-molecular-flow heating due to the low-perigee passage at an inclined angle to the flight path and as a result that the telemetry temperatures were higher than estimated. Equation (15) shows that the temperature increase of the surface is influenced by the emissivity of the surface. Since the values of ϵ_{TH} for the forward shell and steel-covered-grid detectors were much higher than that of the pressure cells, the temperature of these components would be expected to be generally lower. This fact is shown to be the case from the flight data of figure VI-10 and also by the steel-covered-grid-detector data shown in reference VI-3.

In figure VI-10, there is a noticeable fluctuation in the temperature of a number of components with time. This fluctuation can be explained as follows: The orbit is approximately fixed in space, while the Minitrack stations move relative to the orbit path because of the earth's rotation. Thus, the true anomaly of the satellite, as it passes over a given longitude increases by about 24° per orbit. This effect is shown in figure VI-12. Since most of the temperature data gathered from Explorer XIII and shown in figure VI-10 were read out by Minitrack stations at approximately the same longitude, between $\Delta t = 20$ and $\Delta t = 46$ hours, the given temperature history over a 24-hour period corresponds to actual temperature cycling of the components as the satellite completes one orbital revolution.

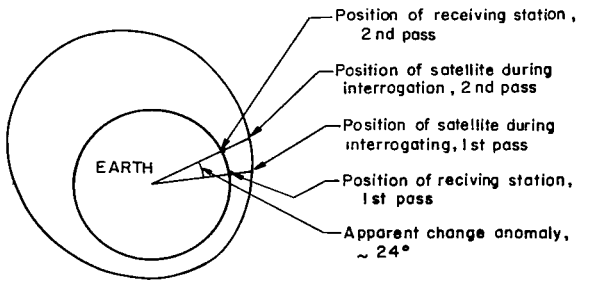

Figure VI-12.- Change in anomaly of successive passes of satellite over a station.

Factors demonstrating that this effect is the predominant cause of these fluctuations are:

1. The period of the fluctuation is 24 hours.

2. The amplitude of the fluctuation is roughly equal that calculated for each component. (For the pressure cells this is approximately 20° F as shown in fig. VI-7.)

3. Temperature changes in figure VI-11 are rapid when the satellite is interrogated near perigee.

4. Since the satellite revolves about the earth in the same direction as the earth rotates, an increase in time in figure VI-10 corresponds to an increase in true anomaly.

From these considerations, it is apparent that data of the type shown in figure VI-11 could provide a typical one-orbit-pass temperature history if allowances were made for the change in orbital elements over a 24-hour period. A close study of predicted temperature histories for Explorer XIII made by using the previous considerations, verifies that the fluctuations in the temperature histories shown in figure VI-11 are due to the normal temperature fluctuations encountered in one orbital pass, with the effects of rapidly changing orbital elements superimposed on it.

The orbital characteristics of Explorer XIII were also used to determine (by the method of ref. VI-1) the percent time in sunlight for correlation with predictions. These results are shown in figure VI-13. Excellent agreement with predictions is indicated for the initial orbits with increasing rate of decay of percent time in sunlight with increasing orbit passes. This decrease was found to be associated with the decrease in apogee altitude. Since the apogee was occurring in sunlight, the decrease in apogee altitude manifested itself as a decrease in percent time in sunlight.

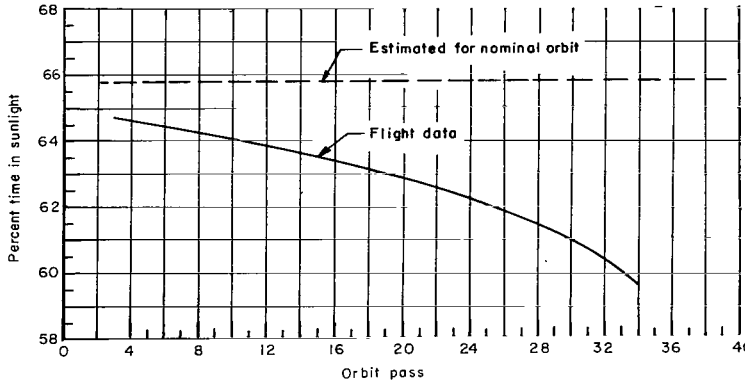

Figure VI-13.- Comparison of estimated and actual percent time in sunlight.

Flight data for Explorer XIII showed a spin rate of 178 rpm during burning and for a short period after burnout of the last stage. This value was 22 rpm less than the expected value (fig. VI-6). It was not possible with the instrumentation used to determine the decay of the spin rate accurately over such a short lifetime, although it would have been possible to determine the time of transition from stable to tumbling spin had the lifetime of the satellite been longer.

SECTION V - CONCLUDING REMARKS

Examination of the temperature data recorded during the lifetime of Explorer XIII indicates surface temperatures and telemetry temperatures which were higher than expected based on calculations for the nominal orbit but were still within the prescribed limits. An analytical study indicated that the high flight temperatures could reasonably be attributed to the existence of free-molecular-flow heating at the low perigee. This heating source would not have been present had the Explorer XIII orbit been as expected.

SECTION VI - REFERENCES

VI-1. Hastings, Earl C., Jr., Turner, Richard E., and Speegle, Katherine C.: Thermal Design of Explorer XIII Micrometeoroid Satellite. NASA TN D-1001, 1962.

VI-2. Morris, J. A., and Byrd, R. J.: Ballistic Performance and Outgassing Studies of X248-A9 Rockets at Simulated Altitude Conditions. AEDC-TN-60-229 (Contract No. AF 40(600)-800 S/A 11(60-110)), Arnold Eng. Dev. Center, Dec. 1960.

VI-3. Staff of the Lewis Research Center: Micrometeoroid Satellite (Explorer XIII) Stainless-Steel Penetration Rate Experiment. NASA TN D-1986, 1963.

VI-4. Eckert, E. R. G., and Drake, Robert M., Jr.: Heat and Mass Transfer. Second ed., McGraw-Hill Book Co., Inc., 1959.

VI-5. Moulton, Forest Ray: An Introduction to Celestial Mechanics. Second rev. ed., The Macmillan Co., c.1914.

VI-6. McLachlan, N. W.: Bessel Functions for Engineers. Clarendon Press (Oxford), 1934.

VI-7. Minzner, R. A., Champion, K. S. W., and Pond, H. L.: The ARDC Model Atmosphere, 1959. Air Force Surveys in Geophysics No. 115 (AFCRC-TR-59-267), Air Force Cambridge Res. Center, Aug. 1959.